Molecular Dynamics Simulations of Methane Hydrate by Means of the Five-Body TIP5P-Ewald Model

Motohiko Tanaka
Innovative Energy Science and Engineering, Chubu University, Japan.

December 19, 2023

Abstract

Microwave heating of methane hydrate is studied with electrostatic molecular dynamics simulations by the five-body rotation coordinate system with the TIP5P-Ewald water model. The structure I of methane hydrate is constructed. When the methane hydrate of density 0.91 $\mathrm{g/cm^3}$ and a temperature 273 K is exposed to microwave electric fields of 10 GHz, it is dynamically unstable and collapses to be liquid after a certain period of irradiation. The period of a collapse time in this model is $1.7\times10^6\tau$ and the temperature increase is $\Delta T\cong 61$ degrees, where the external electric field is 3×10^7V/cm (i.e. 0.3 V/Å) and $\tau=1\times10^{-14}$ s. The high pressure regime of density $0.936\mathrm{g/cm^3}$ becomes stable at the temperture 273 K. The unstable methane hydrate at the 1 atm pressure corresponds to 1.3×10^{-2} s in the 1,000 V/cm power of microwave devices.

Subjects: Chemical Physics (physics.chem-ph)
http://physique.isc.chubu.ac.jp/ Density scaling of microwaves for rotation coordinate system

1 Introduction

The natural gas resources of methane hydrate that are found in permafrost and the sea floor of the earth may be calling public attention [1]. Methane hydrate is a solid or liquid material and is a light electrolyte like ice. The production of methane from methane hydrate, however, will make one order of magnitude more climate warmings than carbon deoxide by greenhouse effects [2, 3].

Methane hydrate has a density of 0.91 $\mathrm{g/cm^3}$ at an atmospheric pressure and 0.95 $\mathrm{g/cm^3}$ for an elevated pressure. Methane hydrate dissociates to about 220 ml of methane gas against 1 g water at 1 atm and 273 K. It is stable at pressures higher than 0.1 MPa at 193 K and 2.3 MPa at 273 K. There are three states of methane hydrates [1, 4]. System I has 46 H_2O molecules that form 5^12 and $5^{12}6^2$ cages containing the guest molecules CH_4 and CO_2. System II has 136 H_2O molecules that form 5^{12} and $5^{12}6^4$ tetragonal cages containing oxygen and other molecules. Both systems have cubic lattices. The hexagonal system H has 5^{12}, $5^{12}6^{16}$, and $4^35^66^3$ polyhedron cages of the C_6H_{14} molecules, which exist as a hexagonal lattice.

High-pressure experiments on methane hydrate have been performed using a diamond-anvil cell [5]. Experiments below the melting point of ice surveyed energetically for hydrates. The stability

of hydrates in the thermodynamic instability of the ice Ih clathrate has been discussed [6]. Many traditional equations of state have been utilized to describe thermo-physical properties and phase equilibrium [7]. The multi-scale phase diagram of the Gibbs-Helmholtz constrained equation of state for methane hydrate has been tabulated by density for given pressures and temperatures [8, 9].

The diffusion coefficients and dielectric relaxation properties of water, i.e., the response of electric dipoles to a given initial impulse, have been studied theoretically [10]. The heating and diffusion of water under high-frequency microwaves and infrared electromagnetic waves have been investigated by molecular dynamics simulations using elaborated point-charge models [11]. Molecular dynamics simulation of the ice nucleation and growth process leading to water freezing has been executed [12].

Concerning the microwave heating of water, ice and saline solution, molecular dynamics simulations have been the first publication as microwave heating of water [13]. They have shown that: (i) water in the liquid phase is heated by excitation of water electric dipoles, which is delayed from the microwave electric field, and absorbed the total microwave power; (ii) hot water gains significantly less heat than the water at room temperature because of smaller phase lags due to less friction; (iii) water in the ice phase is scarcely heated because the electric dipoles can not rotate due to the tightly hydrogen-bonded ice crystal; (iv) dilute saline solution gains significantly more heat than pure water because of the rapid heating of salt ions, especially that of the large salt ions Cl^- and Na^+.

Molecular dynamics employing the density functional method (DFT) to simulate the THz range of electromagnetic wave have been constructed [14]. They have shown, by the self-consistent atomic forces [15], that: (i) liquid water molecules in the electric field has excited rotational motions, as water molecules in the cages can not make free translation motions; (ii) the electron energy is about twice the kinetic energy of the water molecules, which results from the forced excitation of the molecules by the electromagnetic THz external field.

The main simulation goal of the rotation coordinate system with the TIP5P-Ewald model is the following. Is the methane hydrate by microwave irradiation at a normal pressure continued as a crystal or liquid beyond 273 K ? How is the stable and unstable boundary at 273 K located with the density of methane hydrate at the TIP5P-Ewald model ?

The rest of this paper is organized as follows. The methodology of molecular dynamics with equations of motion and forces is written in Section 2.1. The procedures of the five-body water model are given in Section 2.2. Modeling of present simulations is given in Section 3.1, and heating and collapse of methane hydrate are shown in Section 3.2. The microwave devices of 1,000 V/cm are estimated in Section 3.3. A summary is provided in Section 4. The equations of long-range Coulombic interactions are explained in Appendix A.

2 Methodology of molecular dynamics by the TIP5P-Ewald model

2.1 General equations of motion and forces

Crystal structures are fundamental aspects of solid-state physics [16] which may be melted to liquid for elevated temperatures. Molecules of ice and liquid water are within such categories. Four basic quantities in the CGS units system are used to derive the Newtonian equation of motion which are,

(i) time $\tau = 1 \times 10^{-14}$ s, (ii) the length 1 Å= 1×10^{-8} cm, (iii) mass of water $M_0 = 3.0107 \times 10^{-23}$ g, and (iv) electronic charge $e = 4.8033 \times 10^{-10}$ esu (1.6022×10^{-19} C in the international units system). Then, one has the three-dimensional electrostatic version of equations of motion which are written as [13, 17],

$$M_j \frac{d\boldsymbol{V}_j}{dt} = -\nabla \left\{ \Phi_F(\boldsymbol{R}_j) + \sum_{k=1}^{N\star} \left[A/r_{jk}^{12} - B/r_{jk}^{6} \right] \right\} + q_j E \sin \omega t \, \hat{x}, \tag{1}$$

$$\frac{d\boldsymbol{R}_j}{dt} = \boldsymbol{V}_j. \tag{2}$$

The first term of the right-hand side of Eq.(1) is the Coulombic potential $\Phi_F(\boldsymbol{R}_j)$, and the second term is the Lennard-Jones potential. Here, $\boldsymbol{R}_j$ and $\boldsymbol{V}_j$ are the position and velocity of j-th molecule, respectively, M_j and q_j are the mass and charge, respectively, t is the time, and ∇ is the space derivative. The quantity $\boldsymbol{r}_{jk} = \boldsymbol{r}_j - \boldsymbol{r}_k$ is the particle spacing between the j-th and k-th atoms. Also, the symbol $\sum^{\star}$ of Eq.(1) means to take the summation of the oxygens, and the symbol $\sum^{\bullet}$ of Eq.(4) in the paragraph later is that of the hydrogens. A and B are the coeffcients of Lennard-Jones potential, respectively, with $A = 4\varepsilon\sigma^{12}$ and $B = 6\varepsilon\sigma^{6}$ where ε is the depth of the potential well and σ is the distance at which the particle potential energy bocomes zero.

The external electric field E points to the x direction and has the sinusoidal form $\sin \omega t$ where the frequency f is $\omega = 2\pi f$. The time step is $\Delta t = 0.025\tau$ (i.e., 2.5×10^{-16}s). In a time marching fashion, the current step of $\boldsymbol{R}_j$ and $\boldsymbol{V}_j$ is forwarded to the next time step. When a sufficient amount of time has elapsed, one analyzes the time development.

To represent the crystal system with high accuracy, one has to separate the Coulombic forces $\boldsymbol{F}(\boldsymbol{R}_j) = -\nabla\Phi_F(\boldsymbol{R}_j)$ that occur in the short-range and long-range interactions [18, 19, 20],

$$\boldsymbol{F}(\boldsymbol{R}_j) = \boldsymbol{F}_{SR}(\boldsymbol{R}_j) + \boldsymbol{F}_{LR}(\boldsymbol{R}_j). \tag{3}$$

The short-range interactions are written as,

$$\boldsymbol{F}_{SR}(\boldsymbol{R}_j) = \sum_{k=1}^{N\bullet} q_j q_k \Big[\Big(\frac{\mathrm{erfc}(r_{jk})}{r_{jk}} + \frac{2\alpha}{\sqrt{\pi}} \Big) \exp(-(\alpha r_{jk})^2)/r_{jk}^2 \Big] \boldsymbol{r}_{jk}, \tag{4}$$

where the Gauss complimentary error function is

$$\mathrm{erfc}(r) = \frac{2}{\sqrt{\pi}} \int_r^{\infty} \exp(-t^2) dt. \tag{5}$$

The α value, a minimization factor, is discussed later.

A primary factor in the long-range interactions is the charge density, $\rho(\boldsymbol{R}_j) = \sum_k q_k S(\boldsymbol{R}_j - \boldsymbol{R}_k)$, which is the near-site grid sum with $S(\boldsymbol{0}) = 1$, $S(\infty) \to 0$. Then, the grid summation is converted to the k-space by a Fourier transform $FT^{-1}[...]$. Here, $\rho(\boldsymbol{R}) \to \rho_k(\boldsymbol{k})$ with $\boldsymbol{k} = 2\pi\boldsymbol{n}/L$, n the integers ≥ 0, and L the length. The inverse Fourier transform to return to the coordinate space is executed by the folding operations $FT[...]$,

$$\boldsymbol{F}_{LR}(\boldsymbol{R}_j) = -FT \Big[i\, q_j (dn(n_x), dn(n_y), dn(n_z)) G(n_x, n_y, n_z)\, \rho_k(\boldsymbol{k}) \Big], \tag{6}$$

$$dn(n_\gamma) = n_\gamma - dnint(n_\gamma/M_\gamma) M_\gamma \quad (\gamma = x, y, z). \tag{7}$$

The expressions for the $G(n_x,n_y,n_z)$, $\boldsymbol{K}(n_x,n_y,n_z)$ and $\Delta(n_x,n_y,n_z)$ functions are given in Appendix A. The α value is determined by minimizing the errors of both the short-range and long-range interactions of the electric fields [21]. The value is $\alpha = 0.203$ for the total number of 3^3 methane hydrates.

The five-body molecules are used for water which is known as the TIP5P-Ewald model. A four-water molecule is specified to calculate positive two hydrogens $q_H = 0.241e$ and negative two hydrogens $q_L = -0.241e$ with e the electron charge. The angle and bond, respectively, are $\psi_1 = 104.52^\circ$, $r = 0.9572$ Å for the H sites and $\psi_2 = 109.47^\circ$, $r = 0.7$ Å for the dummy L sites whose dynamics motion is not counted. The fifth oxygen atom $q_O = 0$ is to correlate with adjacent molecules using the Lennard-Jones potential $\Psi(r) = A/r^{12} - B/r^6$. The factors of the TIP5P-Ewald water model are $A = 3.8538 \times 10^{-8}$ erg Å^{12} and $B = 4.3676 \times 10^{-11}$ erg Å^6 [22]. The classic mechanics and related topics are written in the Goldstein's book [23].

2.2 Procedures of the translation and rotation coordinate system

2.2.1 The summary of the five-body water model

A) Five sites are one oxygen of O site, hydrogens of H_1 and H_2, and negative hydrogen virtual sites of L_1 and L_2. Their charges are 0, $0.241e$, $0.241e$, $-0.241e$ and $-0.241e$, respectively. The L_1 and L_2 are called the dummy sites.
B) Separate the translational coordinate $\boldsymbol{R}_j$, $\boldsymbol{V}_j$ for molecules ($j = 1, N/5$) from the rotation coordinate $\boldsymbol{r}_i = (x_i, y_i, z_i)$ of atoms ($i = 1, N$) for the five sites. The separation is done at the starting step only; once determined at $t = 0$, they become constant in time.
C) The half time step for the molecules is first executed for a predictor step, and the full time step is made in advancement of time for a corrector step.
D) Before the end of the cycle, the forces are calculated by atomic positions. The dummy sites at L_1 and L_2 are obtained trigonometrically by vector products of O, H_1 and H_2 sites.
E) After correction of quaternions, the kinetic and Coulombic energies are calculated, and go to the beginning of the cycle. The leap-frog method is used for the plasmas and water.

2.2.2 A la carte procedures of the five-body water model

Each step of the simulation cycle of five-body molecules is written, which is (i) translational motion (Step 1), (ii) rotational motion (Steps 2-4), and (iii) the addition of the fields (Steps 5-8).
(0) An extra procedure only at the first time step. Read positions $\boldsymbol{r}_i$ and quaternions $\boldsymbol{q}_j$ from files by "*read*(17) x_i, y_i, z_i" with $i = 1, 2, 3, 6, 7, 8, ...$ where L_1 and L_2 points are defined by the vector products specified in the item D). Also, read the file by "*read*(30) $e_{0j}, e_{1j}, e_{2j}, e_{3j}$" ($j = 1, N/5$).
(1) The position $\boldsymbol{R}_j$ and velocity $\boldsymbol{V}_j$ of each molecule ($j = 1, N/5$) are advanced by summation over five sites of forces $\boldsymbol{F}_k$ ($k = 1, N$) for the translational motion,

$$d\boldsymbol{V}_j/dt = (1/m_j) \sum_{k=1}^{5} \boldsymbol{F}_k, \;\; d\boldsymbol{R}_j/dt = \boldsymbol{V}_j. \tag{8}$$

(2) The rotation coordinate of steps 2) to 5) are made for half a time steps $\Delta t_1 = \Delta t/2$ by prediction, and the next time for a full time step $\Delta t_2 = \Delta t$ by correction. The angular momentum of rotational

motion is calculated at a time step Δt_1 or Δt_2 by summation over the torque of five sites,

$$d\boldsymbol{L}_j/dt_n = \sum_{k=1}^{5} (y_k F_k^z - z_k F_k^y, z_k F_k^x - x_k F_k^z, x_k F_k^y - y_k F_k^x). \tag{9}$$

(3) The angular frequency $\omega_{j,\alpha}$ is connected to the angular mementum and inertia moment $Im_{j,\alpha}$ with $\alpha = x,y,z$ and the matrix $A_{\alpha,\beta}$ are,

$$\omega_{j,\alpha} = (A_{\alpha 1} L_x + A_{\alpha 2} L_y + A_{\alpha 3} L_z)/Im_{j,\alpha}, \tag{10}$$

$$\begin{array}{lll} A_{11} = e_0^2 + e_1^2 - e_2^2 - e_3^2, & A_{12} = 2(e_1 e_2 + e_0 e_3), & A_{13} = 2(e_1 e_3 - e_0 e_2), \\ A_{21} = 2(e_1 e_2 - e_0 e_3), & A_{22} = e_0^2 - e_1^2 + e_2^2 - e_3^2, & A_{23} = 2(e_2 e_3 + e_0 e_1), \\ A_{31} = 2(e_1 e_3 + e_0 e_2), & A_{32} = 2(e_2 e_3 - e_0 e_1), & A_{33} = e_0^2 - e_1^2 - e_2^2 + e_3^2. \end{array} \tag{11}$$

(4) The time derivative of quaternion $\boldsymbol{q}_j = (e_0, e_1, e_2, e_3)$ is given by the angular frequency by,

$$d\boldsymbol{q}_j/dt_n = (1/2)\Delta t_n \begin{pmatrix} -e_1\omega_x - e_2\omega_y - e_3\omega_z \\ e_0\omega_x - e_3\omega_y + e_2\omega_z \\ e_3\omega_x + e_0\omega_y - e_1\omega_z \\ -e_2\omega_x + e_1\omega_y + e_0\omega_z \end{pmatrix}. \tag{12}$$

(5) Get a rotation matrix $A_{\alpha\beta}(e_0, e_1, e_2, e_3)$ in half a time steps for prediction and go back to Step 2. In the correction step, it is calculated for a full time step and go to Step 6.
(6) The three sites $\boldsymbol{r}_i$ and the position $\boldsymbol{R}_j$ are connected by,

$$\boldsymbol{r}_i = \boldsymbol{R}_j + \begin{pmatrix} A_{11} & A_{21} & A_{31} \\ A_{12} & A_{22} & A_{32} \\ A_{13} & A_{23} & A_{33} \end{pmatrix} \begin{pmatrix} x_i \\ y_i \\ z_i \end{pmatrix}. \tag{13}$$

The positions of dummy sites L_1 and L_2 are calculated by the vector product from the known three sites of O, H_1 and H_2.
(7) The forces of positions are calculated from Coulombic and Lennard-Jones potentials using the five sites.
(8) Correction to a normalization of quaternions is made at every 10 steps. Go to the new time step of Step 1.

Note that a time step is important and it will be $\Delta t = 0.025\tau$ or less by the time advancing scheme; otherwise the explicit code will be inaccurate or go to overflow.

3 Simulations of methane hydrate by the TIP5P-Ewald model

3.1 Simulation modeling

To represent electrostatic effects for water molecules, one may adopt the three-body model [24, 25], or various four-body to five-body models [26]. Although the three-body model has a lower temperature problem than the real one, it has a stable symplectic integrator scheme in the coordinate

Table 1: The run series of Runs A's and Run B1, fixed density (g/cm^3), electric field (V/Å), microwave heating rate in linear and nonlinear phases (W_0/τ) with W_0 the initial kinetic energy of methane hydrate, the run time before the collapse, and guest molecules. The kinetic energy increases and collapses for all Run A's runs. (For an initial time $t = -5.0 \times 10^4 \tau \to 0$ in each run, the $E = 0$ phase is not included* in Table 1.)

series	density	E	heating rate*	run from $t = 0$	guest molecules
A1	$0.912 g/cm^3$	0.30 V/Å	$3.0 \times 10^{-7} W_0/\tau$	$1.7 \times 10^6 \tau$ collapsed	CH_4
A2	$0.912 g/cm^3$	0.35 V/Å	$1.3 \times 10^{-6} W_0/\tau$	$2.3 \times 10^5 \tau$ collapsed	CH_4
A3	$0.912 g/cm^3$	0.40 V/Å	$1.6 \times 10^{-5} W_0/\tau$	$1.3 \times 10^4 \tau$ collapsed	CH_4

Table 2: The run series, fixed density (g/cm^3), electric field (V/Å), microwave heating rate in linear and nonlinear phases (W_0/τ), the run time before the collapse, and guest molecules. The volume of simulations are different from the high density case Run B1, the normal density case Run A2, to the low density case Run B3. (For an initial time $t = -5.0 \times 10^4 \tau \to 0$ in each run, the $E = 0$ phase is not included* in Table 2.)

series	density	E	heating rate*	run from $t = 0$	guest molecules
B1	$0.961 g/cm^3$	0.35 V/Å	$1.6 \times 10^{-7} W_0/\tau$	$3.1 \times 10^5 \tau$ running	CH_4
B2	$0.936 g/cm^3$	0.35 V/Å	$2.0 \times 10^{-7} W_0/\tau$	$3.4 \times 10^5 \tau$ running	CH_4
A2	$0.912 g/cm^3$	0.35 V/Å	$1.3 \times 10^{-6} W_0/\tau$	$2.3 \times 10^5 \tau$ collapsed	CH_4
B3	$0.869 g/cm^3$	0.35 V/Å	$6.5 \times 10^{-6} W_0/\tau$	$0.8 \times 10^4 \tau$ collapsed	CH_4

space [27, 28]. The microwave heating and collapse of methane hydrate were studied using the three-body SPC/E model [29]. The five-body models are currently widely used, but there occurs a unrealistic drift to increase the kinetic energy with a time rate $\Delta W_{dr}/\Delta\tau = 1.6 \times 10^{-7} W_0/\tau$ for the null external electric field. The kinetic energies of Run A's and Run B's in Table 1 and Table 2 are subtracted from the tilted baselines.

The initial structure of methane hydrate is installed by the Genice program on the Linux system [30, 31]. The size of structure I methane hydrate has about 12 Å as the crystal structure. A total of 3^3 methane hydrates exists in the three-dimensional water system. The Lennard-Jones potential parameter for water was argued in Sec.2.2. A system of guest molecules of CH_4 which are the united atoms is used for the Lennard-Jones potential in the second term on the righthand side of Eq.(1). ε_{ij} and σ_{ij} are the two-particle interaction potential and the radius of the molecule, respectively, and the potential coefficients are $\varepsilon_{CH_4} = 0.39$ kJ/mol and $\sigma_{CH_4} = 3.82$ Å [32]. In order to perform the molecular dynamics simulation, the frequency is set to 10 GHz ($f = 2\pi \times 10^4/\tau$). The external electric field is changed from $E = 0.30$V/Å for Run A1 to $E = 0.40$V/Å for Run A3 in normal density of $0.912 g/cm^3$.

Also, the external electric field $E = 0.35$V/Å is done for high density of $0.961 g/cm^3$ in Run B1, $0.936 g/cm^3$ in Run B2, and for low density of $0.869 g/cm^3$ in Run B3. The cell size in each direction is 36.01 Å in normal Run A's simulations, that of high density Run B1 is 35.43 Å and Run

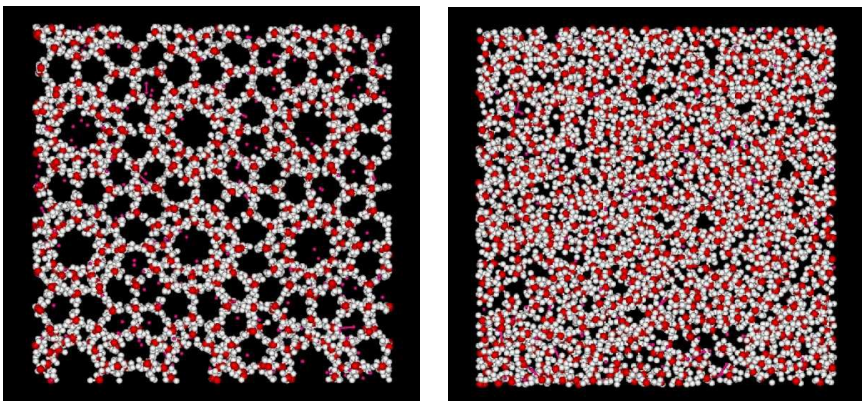

Figure 1: (Left) Methane hydrate of the H (white), O (red), and CH_4 (small red) molecules having density of 0.912 g/cm^3 and the external electric field $E = 0.30$ V/Å before collapse at the time $t = 1.60 \times 10^6 \tau$. (Right) Distortion of the methane hydrate in liquid under an applied microwave field observed at $t = 1.65 \times 10^6 \tau$.

B2 is 35.71 Å, respectively, and that of low density Run B3 is 36.63 Å.

3.2 Dependence of heating on microwave fields

The heating of methane hydrates is done under the application of microwave fields. In the heating described, the volume is assumed to be constant. The hydrate used in this simulation is a normal pressure case (1 atm, Run A's), and the density is 0.912 g/cm^3 [1, 9]. The run has an initial temperature of 273 K of the crystal. The translational and rotational motions are solved for the water molecules as stated in Sec.2. The kinetic energy of the water molecule is $W_{ekin} = (1/2)\sum_{s,j}(M_0 V_{s,j}^2 + I_{s,j}\omega_{s,j}^2)$, where $V_{s,j}$ and $\omega_{s,j}$ are the velocity and angular frequency, respectively, of the s directions ($s = x, y, z$) and the j-th particle. M_0 is the mass of water, and $I_{s,j}$ is the inertia moment.

After an initial quiet phase of $t = -5 \times 10^4 \tau - 0.$ is passed, the external electric field of microwaves is applied in the x-direction. The translational and rotatinal energies of water are almost equal as expected, and Coulombic and Lennard-Jones energies increase in time. The kinetic energies of the water and CH_4 molecules increase over time, but the water and CH_4 (unified atom) molecules behave similarly in the linear phase on the left panels of Fig.1.

The nonlinear growth of methane hydrate occurs for the time $t > 0$ of Run A1. The increase in the energy of the water is $\Delta W/\Delta\tau \cong 3.0 \times 10^{-7} W_0/\tau$. The CH_4 molecules without any charges are inert to microwaves, but they interact with water molecules. The energy increases in the Lennard-Jones potential, which was close to the water case. The temperature increase before the microwave collapse for Run A1 is $\Delta T \cong 61$ degrees. The total energy of the kinetic energies of water and CH_4 become very large at $t > 1.7 \times 10^6 \tau$, as depicted in Fig.2. The explosive growth suddenly collapses, and the Lennard-Jones energy decreases chaotically. Methane hydrate turns to be the liquid phase, as the right panel of Fig.1.

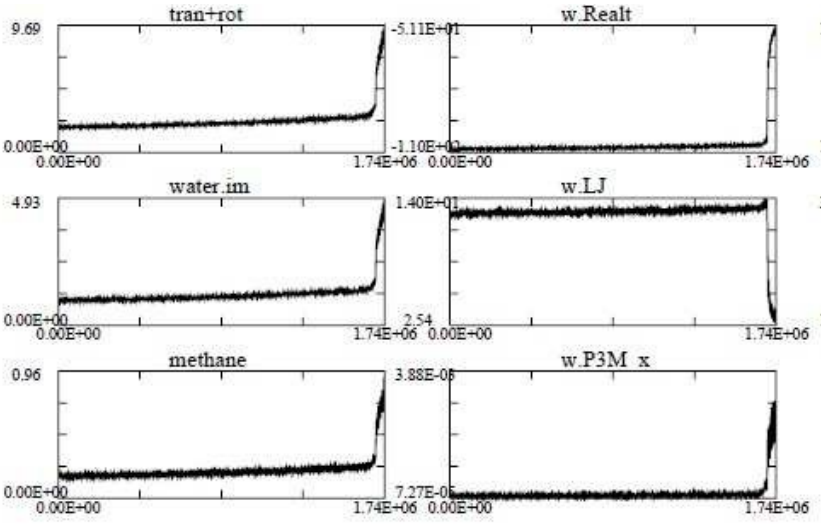

Figure 2: Microwaves are applied to methane hydrate with density of 0.912 g/cm^3, the initial temperature $T = 273$ K and the external electric field $E = 0.30$ V/Å. Left: The kinetic energy of translation+rotation, that of rotation, that of CH_4 (top to bottom, respectively). Right: The short-range Coulomb interaction energy, the Lennard-Jones potential energy, and P3M energy (top to bottom, respectively). The abscissa is linearly scaled in all plots. The kinetic energy of water increases with a time rate of $\Delta W/\Delta\tau = 3.0\times10^{-7}W_0/\tau$, and the short and long-range energies eventually collapse to be liquid at the time $t \cong 1.7\times10^6\tau$, whereas the Lennard-Jones energy decreases at the same time (the initial $E = 0$ phase of $5\times10^4\tau$ is included in this figure).

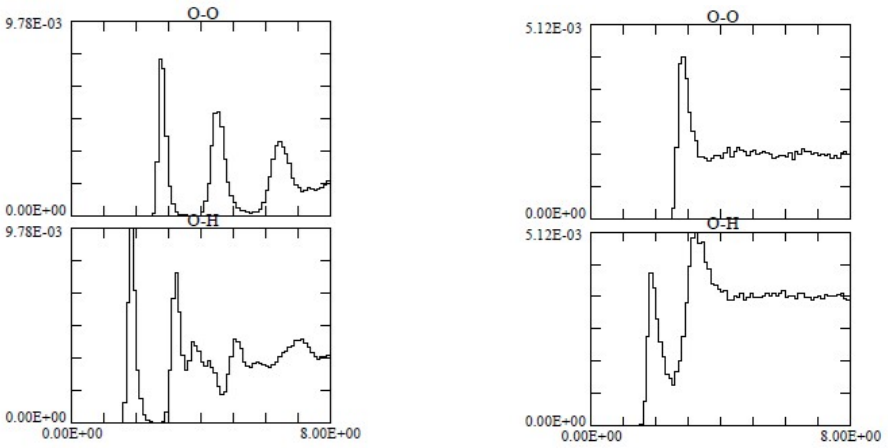

Figure 3: The pair distribution functions between the O-O atoms (top) and O-H atoms (bottom) of the methane hydrate for the density 0.912 g/cm^3 and the external electric field $E = 0.30$ V/Å. The time is before the collapse at $t = 1.60\times10^6\tau$ (left), and after the collapse at $t = 1.65\times10^6\tau$ (right). The three peaks for the O-O atoms show that the atoms have almost aggregated by the collapse in the right panel, and the two giant peaks indicate the O-H atoms.

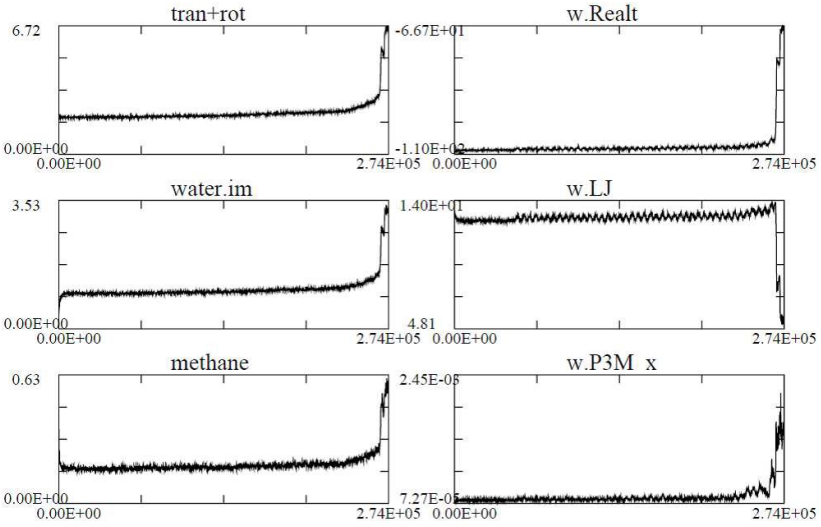

Figure 4: Microwaves are applied to methane hydrate with density of 0.912 g/cm^3, the initial temperature $T = 273$ K and the external electric field $E = 0.35$ V/Å of Run A2. Left: The kinetic energy of translation+rotation, that of rotation, that of CH_4 (top to bottom, respectively). Right: The short-range Coulomb interaction energy, the Lennard-Jones potential energy, and P3M energy (top to bottom, respectively). The abscissa is linearly scaled in all plots. The kinetic energy of water increases with $\Delta W/\Delta\tau = 1.3\times10^{-6}W_0/\tau$, and the short and long-range energies collapse to be liquid at the time $t \cong 2.3\times10^5\tau$ (the initial phase with $E = 0$ is included in this figure).

The pair distribution functions of the O-O and O-H atoms are shown in Fig.3 for the methane hydrate. Their times are corresponding to before and after the collapse around $\tau \cong 1.7\times10^6\tau_0$. Well separated peaks in the 8 Å regions can be identified as a crystal before the collapse on the top and bottom panels of the left side, respectively. However, one has only one peak as liquid after the collapse, which is entirely buried in the $r > 3$ Å region of the O-O distribution function. Two peaks are seen with curtains in the O-H functions of the right panel.

In the external electric field $E = 0.35$ V/Å of Run A2, methane hydrate stays in a linear phase shown in Fig.4, which goes into a nonlinear phase for $t > 1.9\times10^5\tau$ similarly to the case of Run A1. After the nonlinear phase, it is then collapsed at the time $t \cong 2.3\times10^5\tau$. The external electric field $E = 0.40$ V/Å of Run A3 is made large, and the heating rate becomes very large as $1.6\times10^{-5}W_0/\tau$. There is a short nonlinear phase before its collapse at $t \cong 1.3\times10^4\tau$.

3.3 Dependence of heating on high and low densities

Methane hydrate of the high density of 0.961g/cm^3 with increased pressure is started from a new initial condition in Run B1 of Table 2. The tilted baseline in $E = 0$ has been subtracted from the Run B1 value. This high density has been continued where the kinetic energy by microwave heating increases for the small amount by $1.6\times10^{-7}W_0/\tau$ at the time of $3.1\times10^5\tau$. The mediumly high density of 0.936g/cm^3 of Run B2 is also stable whose heating rate is $2.0\times10^{-7}W_0/\tau$ in the TIP5P-

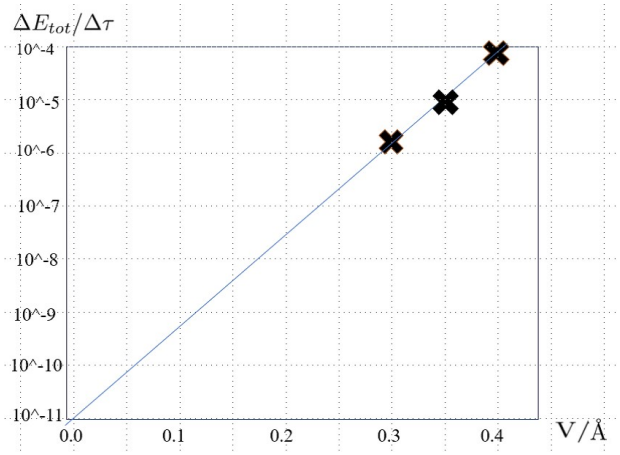

Figure 5: The time derivative of kinetic and potential energies for the external electric field from $E = 0.30$ V/Å (Run A1) to $E = 0.40$ V/Å (Run A3) is extrapolated against the run at $E = 1 \times 10^{-5}$ V/Å = 1,000 V/cm.

Ewald model simulation. The temperature increase is not small by the microwave irradiations, but is finite as about 10 degrees $3 \times 10^5 \tau$ in Run B1 and Run B2. We may then put methane hydrate to the nonlinear and collapse phase in ten times more simulations.

The normal density case of Run A2 was shown unstale and collapsed as Table 1. For the low density of $0.87 \mathrm{g/cm}^3$ with low pressure case, the short heating is observed which is followed by the collapse of methane hydrate.

About the five-body water model of Run A1, it is shown that there is a factor of two the difference of the collapse time of the TIP5P-Ewald model from the short collapse time of the SPC/E model in the same parameters [29].

3.4 The microwave devices of the 1,000 V/cm input power

The normal input power of the microwave devices is estimated. The time derivative of kinetic and potential energies for Run A1 - Run A3 is plotted against the microwave devices of 1×10^3 V/cm in Fig.5. The data of $\Delta E_{tot}/\Delta\tau = 1.5 \times 10^{-6} W_0/\tau$ of Run A1 is shown to be reduced to $0.4 \times 10^{-11} W_0/\tau$, which is dynamically unstable of methane hydrate on the most left side of the figure. The conversion from 10 GHz to 2.45 GHz together becomes the final collapse time as $(1.7 \times 10^6 \times 10^{-14}\mathrm{s}) \times (1.5 \times 10^{-6}/0.8 \times 10^{-11}) \times (10/2.45) \cong 1.3 \times 10^{-2}$ s.

4 Summary

Methane hydrate was simulated by molecular dynamics with periodic boundary conditions. The normal density of 0.91 g/cm^3 represented the sea level condition, and the high density > 0.935 g/cm^3 corresponded to the high-pressure condition at 273 K. The microwave electric field was applied while the volume was held constant. For Run A1, the external electric field was $E = 0.30$V/Å and

the heating rate was $3.0\times10^{-7}W_0/\tau$. The unstable methane hydrate collapsed as liquid for the pressure 1 atm, and the temperture increase was $\Delta T\cong 61$ degrees at $t\cong 1.7\times10^6\tau$.

In the external electric field $E=0.35$ V/Å, methane hydrate collapsed at the time $t\cong 2.3\times10^5\tau$. For Run A3 of $E=0.40$ V/Å, the heating rate was very large as $1.6\times10^{-5}W_0/\tau$, and methane hydrate collapsed shortly at $t\cong 1.3\times10^4\tau$. On the other hand, for the high density of $0.961\mathrm{g/cm}^3$ in Run B1 and also $0.936\mathrm{g/cm}^3$ in Run B2 for the increased pressures, the kinetic energy remained stable and the small microwave heating was obseved. The stable and unstable boundary at the temperature 273 K is expected to be around $0.93\mathrm{g/cm}^3$, which was for the pressure of 2.3 MPa.

The methane hydrate in the devices of $E=$ 1,000 V/cm and the pressure 1 atm was shown to be unstable and collapsed in 1.3×10^{-2} s, which might be consistent with the current microwave ovens.

Acknowledgments

The author thanks Dr. M. Matsumoto of Okayama University for the initial configurations of methane hydrate. The computation is performed by the NEC SX-Aurora TSUBASA and the Intel LX Server of National Institute of Fusion Science in Toki City, Japan.

Appendix A: Long-range Coulombic interactions

The long-range Coulombic interactions $\boldsymbol{F}_{LR}(\boldsymbol{r})$ are defined in the Fourier space using $dn(n_\gamma)$, $G(n_x,n_y,n_z)$, $\boldsymbol{K}(n_x,n_y,n_z)$ and $\Delta(n_x,n_y,n_z)$ functions in Eq.(6), Eq.(7), which are written in the periodic boundary conditions,

$$G(n_x,n_y,n_z)=(2M_xM_yM_z/L^2)\times\Big[dn(n_x)K_x+dn(n_y)K_y+dn(n_z)K_z\Big]/(\Lambda\Delta^2), \tag{A.1}$$

$$\boldsymbol{K}(n_x,n_y,n_z)=\sum_{n_1,n_2,n_3}(n_1,n_2,n_3)\Big\{\exp\Big(-\Big(\pi/(\alpha L)\Big)^2\Big)/\Lambda\Big\}\times \Big(sinc\Big(\frac{n_x+M_xn_1}{M_x}\Big)\Big)^{2P}\Big(sinc\Big(\frac{n_y+M_yn_2}{M_y}\Big)\Big)^{2P}\Big(sinc\Big(\frac{n_z+M_zn_3}{M_z}\Big)\Big)^{2P} \tag{A.2}$$

$$\Delta(n_x,n_y,n_z)=\sum_{n_1,n_2,n_3}\Big(sinc\Big(\frac{n_x+M_xn_1}{M_x}\Big)\Big)^{2P}\times \Big(sinc\Big(\frac{n_y+M_yn_2}{M_y}\Big)\Big)^{2P}\Big(sinc\Big(\frac{n_z+M_zn_3}{M_z}\Big)\Big)^{2P}, \tag{A.3}$$

$$\Lambda=dn(n_x)^2+dn(n_y)^2+dn(n_z)^2. \tag{A.4}$$

The first Brillouin zone should take the summation of $-1\le n_1\le 1$ (the degree is $P=3$), and M_x is the mesh in the x direction; the same procedures should be taken in the other directions due to the tetragonal crystal symmetry. The sinc function is used to account for the long slopes of the $\boldsymbol{K}(n_x,n_y,n_z)$ and $\Delta(n_x,n_y,n_z)$ functions. The index ranges for the $G(n_x,n_y,n_z)$ function are $0\le n_x\le M_x/2$, $0\le n_y\le M_y-1$ and $0\le n_z\le M_z-1$, where M_x, M_y, and M_z are the number of points in the x,y, and z directions, respectively.

References

[1] E. D. Sloan, C. A. Koh, C. Koh, Clathrate Hydrates of Natural Gases, Third Edition, CRC Press (2007).

[2] A. A. Pavlov, J. F. Kastine, L. L. Brown, K. A. Rages, and R. Freedman, J. Geophys. Res., 105, 981-990 (2000).

[3] United State Environmental Protection Agency, Greenhouse Gas Emissions, https://www.epa.gov/ghgemissions/overview-greenhouse-gases.

[4] Methane hydrate mineral data, The Hudson Institute of Mineralogy, http://webmineral.com/data/Methane.

[5] H. Hirai, T. Tanaka, T. Kawamura, Y. Yamamoto, and T. Yagi, Phys. Rev. B, 68, 172102 (2003).

[6] O. S. Subbotin, T. Ikeshoji, V. R. Belosludov, J. Kudoh, R. V. Belosludov, and Y. Kawazoe, J. Physics Conference Series 29, 206 (2006).

[7] G. Soave, Chem. Eng. Sci. 27, 1197 (1972).

[8] A. Lucia, J. Thermodyn., Article id: 238365 (2010).

[9] H. Henley, E. Thomas, and A. Lucia, 92, 1977 (2014).

[10] T. Yamaguchi, S. H. Chong, and F. Hirata, J. Chem. Phys. 116, 2502 (2002).

[11] N. J. English and J. M. MacElroy, J. Chem. Phys. 118, 1589 (2003).

[12] M. Matsumoto, S. Saito and I. Ohmine , Nature, vol. 416, 409 (2002).

[13] M.Tanaka and M.Sato, J.Chem.Phys., 126, 034509 (2007).

[14] M.Tanaka and M.Sato, JMPEE, 42, 62-69 (2008).

[15] J. Izquierdo, A. Vega, L. Balbas, D. Sanchez-Portal, J. Junquera, E. Artacho, J. Soler, and P. Ordejon, Phys. Rev. B. 61, 13639 (2000).

[16] C. Kittel, Introduction to Solid State Physics, Six Edition (Willey, New York 1986).

[17] M. Tanaka and M. Murakami, Computer Physics Commun., 241, 56 (2019).

[18] P. Ewald, Ann. Phys. 369, 253 (1921).

[19] J. Kolafa, and J. W. Perram, Molecular Simulation. 9, 351 (1992).

[20] D. Frenkel and B. Smit, Understanding Molecular Simulation - From Algorithms to Applications, 2nd edition, Academic Press, United Kingdom, 2001.

[21] M. Deserno and C. Holm, J. Chem. Phys. 109, 7694 (1998).

[22] S.W. Rick, J. Chem. Phys. 120, 6085–6093 (2004).

[23] “Classical Mechanics”, H. Goldstein, C. Poolee, J. Safko, 3rd Edition, Pearson Education Inc., England, 2003.

[24] H.C. Andersen, J. Comp. Physics, 52, 24-34 (1983).

[25] H.J.C. Berendsen, J.R. Grigera, T.P. Straatsma, J. Phys. Chem., 91, 6269 (1987)

[26] W.L. Jorgensen, J. Chandrasekhar, J.D. Madura, R.W. Impey, and M.R. Klein, J. Chem. Phys 79, 926 (1983).

[27] E. Forest and R. D. Ruth, Physica, D.43, 105 (1990).

[28] T.Okabe, H.Yamada and M.Goda, Int. J. Mod. Phys. C, 7. 613 (1996).

[29] M. Tanaka, M. Sato, and S. Nakatani, arXiv:1909.01024, Cornell University Library (2019).

[30] M. Matsumoto, T. Yagasaki, H. Tanaka, “GenIce: Hydrogen-Disordered Ice Generator”, Wiley online, https://doi.org/10.1002/jcc.25077.

[31] M. Tanaka, “Water and hydrate simulation by molecular dynamics TIP5P model”, https://github.com/Mtanaka77/; http://www1.w4.mediacat.ne.jp/dphysique/.

[32] A. Venkattraman and A. A. Alexeenko, Physics Fluids, 24, 027101 (2012).